2001 SN$_{263}$ – the contribution of their irregular shapes on the neighbourhood dynamics

G. Valvano [ID],[1]* O. C. Winter [ID],[1] R. Sfair [ID],[1,2] R. Machado Oliveira [ID][1] and G. Borderes-Motta [ID][3]

[1]*Grupo de Dinâmica Orbital e Planetologia, São Paulo State University, UNESP, Guaratinguetá, CEP 12516-410, São Paulo, Brazil*
[2]*Institut für Astronomie und Astrophysik, Eberhard Karls Universität Tübingen, D-72074 Tübingen, Germany*
[3]*Bioengineering and Aerospace Engineering Department, Universidad Carlos III de Madrid, Leganés, E-28911 Madrid, Spain*

ABSTRACT

The first proposed Brazilian mission to deep space, the ASTER mission, has the triple asteroid system (153591) 2001 SN$_{263}$ as a target. One of the mission's main goals is to analyse the physical and dynamical structures of the system to understand its origin and evolution. This work aims to analyse how the asteroid's irregular shape interferes with the stability around the system. The results show that the irregular shape of the bodies plays an important role in the dynamics nearby the system. For instance, the perturbation due to the (153591) 2001 SN$_{263}$ Alpha's shape affects the stability in the (153591) 2001 SN$_{263}$ Gamma's vicinity. Similarly, the (153591) 2001 SN$_{263}$ Beta's irregularity causes a significant instability in its nearby environment. As expected, the prograde case is the most unstable, while the retrograde scenario presents more stability. Additionally, we investigate how the solar radiation pressure perturbs particles of different sizes orbiting the triple system. We found that particles with a 10–50 cm radius could survive the radiation pressure for the retrograde case. Meanwhile, to resist solar radiation, the particles in prograde orbit must be larger than the particles in retrograde orbits, at least one order of magnitude.

Key words: celestial mechanics – minor planets, asteroids: general – planets and satellites: dynamical evolution and stability.

1 INTRODUCTION

Over the past years, several space missions have targeted asteroids to comprehend their formation, evolution, and dynamics since they are the remaining bodies of the inner Solar system. The NEAR-Shoemaker mission was the first spacecraft to orbit the asteroid (433) Eros and ended up touching its surface, being also the first one to land on an asteroid (Veverka et al. 2000; Prockter et al. 2002). The asteroid (25143) Itokawa was imaged by the Hayabusa spacecraft and was the first mission to collect samples from the surface of an asteroid (Fujiwara et al. 2006; Yoshikawa et al. 2015). Similarly, the Hayabusa 2 spacecraft performed a touchdown in 2019 on the asteroid (162173) Ryugu, and the collected samples arrived on Earth in 2020 December (Kawaguchi, Fujiwara & Uesugi 2008; Müller et al. 2017). The OSIRIS-REx mission also plans to return in 2023 a sample collected from the asteroid (101955) Bennu (Lauretta et al. 2015, 2017), another spinning-top shape asteroid as Ryugu. The first space mission intended to demonstrate an asteroid deflection by kinetic impactor is DART (Double Asteroid Redirection Test), and the mission target is the binary near-Earth system Didymos-Dimorphos (Cheng et al. 2016). The multiple system of asteroids is notably attractive for space missions as they can provide a manifold of observational possibilities, investigation of the system origin, and the dynamics involved. Based on these same concepts, the ASTER mission team chose as its target a triple system to be the first Brazilian deep space mission (Sukhanov et al. 2010).

The target of the ASTER mission, the asteroid (153591) 2001 SN$_{263}$, was discovered in 2001 by LINEAR (Lincoln Near-Earth Asteroid Research). However, radar observations from Arecibo in 2008 revealed the asteroid is, in fact, a triple system. The system is composed of the central body called Alpha and two secondary bodies, Beta and Gamma, being Gamma the smallest. Using the same data, Fang et al. (2011) made the best fit for their physical and orbital parameters. Araujo et al. (2012) and Araujo, Winter & Prado (2015), motivated by the ASTER mission announcement, investigated the stability of internal and external regions to the triple system for prograde and retrograde orbits. They made a set of numerical simulations considering the asteroids as spherical bodies and reported regions of stability between them. Prado (2014) plotted the perturbation map for a spacecraft orbiting the triple system. Their results showed that Gamma causes a more significant perturbation in the system, one order of magnitude larger than the perturbation caused by Beta and two orders larger than Alpha's oblateness for particles with a semi-major axis around 2–40 km. Sanchez & Prado (2019) also searched for orbits around the system but considering the solar radiation pressure. They mapped the duration of the orbits considering values of semi-major axis, eccentricity, and inclination. They identified some possibly stable areas and a limit on the size of the spacecraft solar panels for their stable results. In none of these previous works, the actual irregular shape of the bodies was taken into account. Adopting the polyhedral shape model for each asteroid, derived by Becker et al. (2015), Winter et al. (2020) explored the geometric and geopotential topographic of the bodies and the dynamical environment around each system component. They determined 12 equilibrium points for the central body. Also,

* E-mail: giulia.valvano@unesp.br

Table 1. Physical and orbital data of each component of the triple asteroid system (153591) 2001 SN$_{263}$.

Body	Volumetric radius (km)	Density^b (g cm^{-3})	Spin^b (h)	Mass^a (10^{10} kg)	Orbit	Semi-major axis ^{a}	Eccentricity^a	Inclination^a (°)	Orbital period
Alpha	1.25	1.10	3.4256	917.466 ± 2.235	Sun	1.99 AU	0.48	6.7	2.8 yr^c
Beta	0.39	1.00	13.43	24.039 ± 7.531	Alpha	16.63 km	0.015	0.0	6.23 days^a
Gamma	0.22	2.30	16.40	9.773 ± 3.273	Alpha	3.80 km	0.016	14	16.46 h^a

^{a}Fang et al. (2011).
^{b}Becker et al. (2015).
^{c}JPL. website: https://ssd.jpl.nasa.gov/.
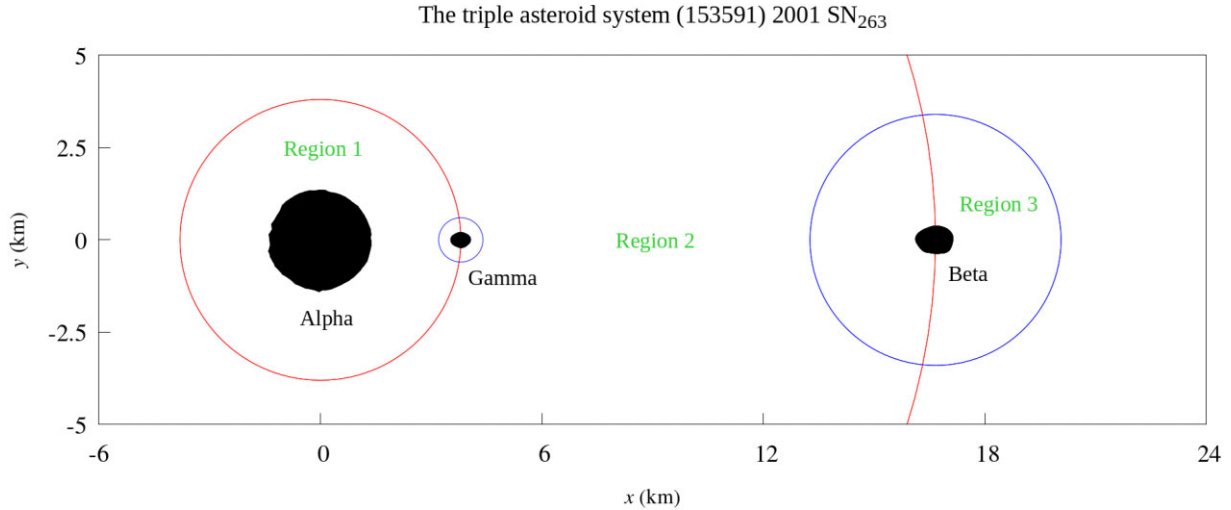
Figure 1. Representation of the triple system (153591) 2001 SN$_{263}$ in the Alpha centred equatorial plane, *xoy*. The red circles represent the orbits of Gamma and Beta and, also, the collision lines for regions 1 and 2. The blue circles represent the Hill's radii of Beta-Alpha (ejection distance for region 3) and Gamma-Alpha.

they found that the particles initially in a cloud around Alpha would fall preferentially on the equatorial bulge and the polar regions.

Considering the singular dynamics and the previous analyses, we aim to investigate the stability of different regions of the system, taking into account the gravitational effects due to irregular shape models of the bodies and the effects the solar radiation pressure as an extension of the results of Araujo et al. (2012), Araujo et al. (2015). First, in Section 2, we present the physical and orbital properties of the system. Then, a set of numerical simulations of discs of test particles in the triple system is presented and discussed in Section 3. In the next section, we add the perturbation of the solar radiation pressure and investigate how this perturbation changes the stability of particles in the system. Next, long-period simulations are presented in the Section 5. Then, we provide the final comments for our results (Section 6).

2 THE TRIPLE ASTEROID SYSTEM (153591) 2001 SN₂₆₃

In this section, we discuss about the orbital and physical properties, and the irregular shape models of the (153591) 2001 SN$_{263}$ bodies.

2.1 Orbital properties

In 2008 February 20, the triple system 2001 SN$_{263}$ reached a distance of 0.066 AU from the Earth and was observed by Arecibo and Goldstone radio telescopes. Based on radar data, Fang et al. (2011) provided orbital fits for the system and the orbital evolution consider-

ing the mutual gravitational perturbation among the asteroids (Fang et al. 2011). The semi-major axes, eccentricities, and inclinations found are given in Table 1, and a representation of the system in the Alpha centred equatorial plane is shown in Fig. 1. The red circles in Fig. 1 represent the orbits of the secondary bodies and the blue circles their respective Hill's radii. The Hill's radii can be used as a parameter to bound the regions where a body is gravitationally dominant. We computed the Hill's radii of Beta and Gamma with respect to Alpha, which are ~3.4 km and ~ 600 m, respectively. Then, we delimit the regions that will be used in our analysis in the same way as was done by Araujo et al. (2012, 2015), since we will compare the stability by regions. Region 1 is delimited as the region interior to Gamma's orbit; region 2 is between Gamma's and Beta's orbits and region 3 is just delimited as the region interior to Beta's Hill's radius.

Besides the orbital elements, Fang et al. (2011) present fits for the pole direction of Beta and Gamma. They stated that about 25 per cent of their adjusts resulted in retrograde orbits (contrary to Alpha's spin). However, they reported that Beta and Gamma are more likely to be prograde. The retrograde result was possible due to a wide range of spin axis orientations for Alpha, though the orbital orientations of the secondary bodies are well defined. Becker et al. (2015) also investigated the 2001 SN$_{263}$ orientation and searched for the best fit for the spin axis of Alpha. They reported an obliquity of about 166° and the spin-axis pole of $(\lambda, \beta) = (309, -80) \pm 15°$, which is similar to the pole orientation reported by Fang et al. (2011). To reproduce a similar Alpha's pole orientation, we considered, for simplicity, the obliquity of Alpha and 270° for the pole's longitude.

2.2 Shape model and physical properties

The 2001 SN$_{263}$ shape model was derived by Becker et al. (2015) from the combination of radar and light curves data taken in 2008 from Arecibo and eight other observatories. The three shape models have equivalent diameters of about 2.5, 0.77, and 0.43 km for Alpha, Beta, and Gamma, respectively. A polyhedron modeled each body with 1148 vertices and 2292 triangular faces. In the same study, Becker et al. (2015) derived a rotational period for each body (Table 1).

Fang et al. (2011) also reported the mass for each asteroid (Table 1). Considering the mass and the volume of the shape models, Becker et al. (2015) estimated a bulk density for the bodies and concluded that the bodies are carbonaceous asteroids of type B. Perna et al. (2014) came to the same conclusion for the B-type classification by comparing the reflectance spectra with laboratory spectra data. They also concluded that the bodies have an organic- and magnetite-rich surface composition, similar to the CI carbonaceous chondrites. The bulk density of Alpha and Beta are similar and compatible with the BCG-types (B-, C-, Cb- and Cg-type) range of about 0.7–1.7 g cm^{-3} (Marchis et al. 2012; Vernazza et al. 2015). However, the Gamma's bulk density is much higher. The grain density of carbonaceous chondrites is approximately 2.42–5.66 g cm^{-3}, with an average of 3.44 g cm^{-3} (Macke, Consolmagno & Britt 2011; Carry 2012; Flynn et al. 2018; Ostrowski & Bryson 2019). Thus, considering the mean value, Gamma must have a porosity smaller than Alpha and Beta if its bulk density is 2.3 g cm^{-3}. This difference may indicate that Gamma could have been originated from a different parental body. If we consider a scenario with a collision between two different parent bodies with different bulk densities (Michel et al. 2020). We also have to consider the spinning-top shape of the central body. After the disruption collision, the aggregate parental body of Alpha may have started to YORP spin-up, resulting in the current diamond shape (Rubincam 2000; Walsh, Richardson & Michel 2008; Sánchez & Scheeres 2016; Walsh 2018).

This diamond shape has larger values of altitude on its equatorial bulge and the polar regions (Fig. 2). We also can see that the mid-latitude regions have lower altitudes. Alpha's shape is characteristic of spinning-top asteroids that are a result of their fast spin (Harris, Fahnestock & Pravec 2009; Hirabayashi et al. 2020). Differently from Alpha, Beta has flattened poles with the lower altitudes located in these regions (see the top and bottom views in Fig. 2 – Beta). The maximum altitudes for this body are in the equatorial extremity. Gamma also has the upper altitudes in its equatorial extremities. However, its poles are not so flat as Beta's ones. We can see in both poles the existence of moderate altitude followed by valleys with lower values (top and bottom views of Fig. 2 – Gamma). Note that Beta has the more considerable relative variation of altitudes, with the maximum reaching about twice the minimum altitude. On the other hand, Alpha and Gamma have a similar relative variation, the ratio between the maximum and minimum altitudes of Alpha is about 1.4, and Gamma is 1.6.

The irregularities in the shapes of the bodies influence their gravitational field. Thus, if we treat the system as a point of mass (or spherical bodies), as done by Araujo et al. (2012, 2015), it may not be a satisfactory approximation. Using the volumetric radius of Alpha (Table 1), we will lose peaks of at least 210 m of altitude. For Beta and Gamma, we will miss about 150 and 50 m, respectively, and, consequently, their irregularities (Fig. 2). So, to identify the contribution due to the irregular format of the system's bodies, in the following sessions, we will present a set of numerical simulations
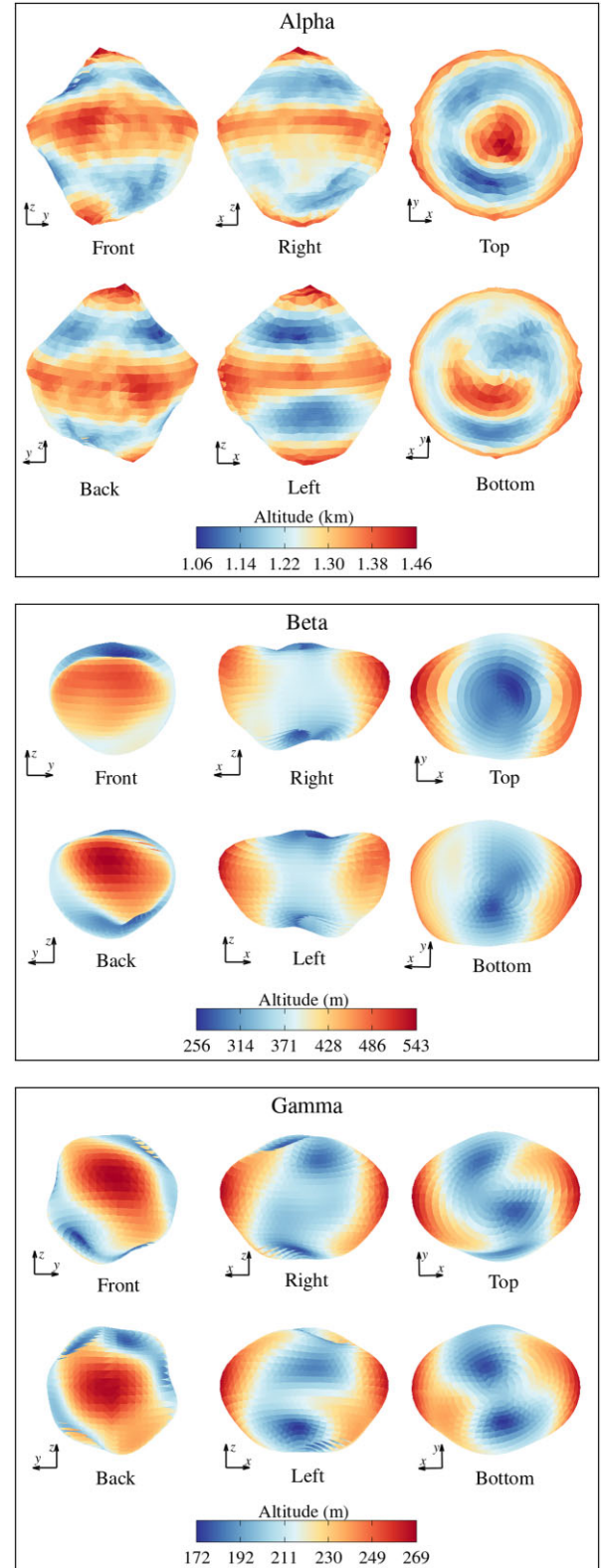
Figure 2. Map of the geometric altitude across the surfaces of Alpha, Beta, and Gamma under different views.

with test particles in the triple system gravitational field to analyse their stability.

3 EFFECTS ON THE NEARBY ENVIRONMENT

The dynamics nearby the system were studied by Araujo et al. (2012, 2015) to identify possible stable regions for a spacecraft or locations for natural objects, such as fragments or dust. Then, they explored the stability of massless particles discs in prograde and retrograde trajectories in the system through a set of numerical simulations considering the triple system, the Sun, Earth, Mars, and Jupiter as a point of mass (or spherical objects) and included the oblateness of Alpha (J_2). The particles were distributed in different regions: between Alpha and Gamma, Gamma and Beta, around Beta, and an outer region with the particles orbiting the triple system.

In this work, our goal is to advance the results of Araujo et al. (2012), Araujo et al. (2015) considering a more realistic scenario. Our main concerns are the effects caused by the irregular shapes of the triple system components on the stability of the particles. Another perturbation that we will consider is the solar radiation pressure, which might be relevant depending on the particle size.

Thus, we performed a set of numerical simulations of test particles using the N-BOM package (Winter et al. 2020). Mascon models computed the gravitational potential of the irregular bodies, the mass of the body is uniformly divided into a tridimensional equally spaced grid (Geissler et al. 1996; Borderes-Motta & Winter 2017). We modeled Alpha using a with 24 328 mass points and Beta with 24 065 grid-points. Since we want to verify how the irregular shape of the bodies interferes with the particle stability, we first reproduced the figures of Araujo et al. (2012, 2015) to make the comparisons. For simplicity, we did not consider the perturbations of the planets since they do not contribute to the stabilization of the particles. Hereinafter, 'standard case' refers to the simulations based on Araujo et al. (2012, 2015), while the 'mascons case' is our solution that takes into account the shape models.

The distribution of the initial conditions of particles was made in pairs of semi-major axis and eccentricity. For regions 1 and 2, the particles were orbiting Alpha with semi-major axes in the intervals [1.4, 3.2] and [4.5, 13.5] km, respectively, while the particles in region 3 were orbiting Beta with semi-major axes between 0.8 and 3.4 km. Each range of the semi-major axis was evenly divided into steps of 200 m, and the eccentricity ranged from 0.0 to 0.5 in steps of 0.05. The inclination for the particles was initially 0° for prograde trajectories and 180° for retrograde trajectories. We consider prograde trajectories the orbits that have the same direction of the angular momentum of the orbited body. In each case, the initial conditions were randomly chosen for the other angular orbital elements.

For each region, we considered a different ejection distance. The ejection distance means that the particle has left its initial region and does not necessarily leave the system. The ejection distance for region 1 was 3.80 km, which corresponds to the semi-major axis of Gamma. Region 2 has an ejection distance of 16.63 km, corresponding to the semi-major axis Beta (Table 1); the Hill's radii of Beta, 3.4 km, delimits the ejection distance for region 3. The system was integrated for 2 yr, and we classified the stability according to the percentage of particles for a given pair (*a*, *e*) that survived (i.e. were not ejected nor collided with a body) the entire time.

Araujo et al. (2012, 2015) also considered a fourth region, external to the triple system, starting from 20 km. However, we did not simulate this region since it is far distant from bodies Alpha and Beta. Therefore, their irregular shape will not interfere significantly with the dynamics of the particles' stability.

### 3.1 Orbits of the triple system components

To study the dynamics of the triple system, we considered Alpha at the system origin and the orbital elements of Beta and Gamma provided by Fang et al. (2011) (Table 1), with the other angular elements set as zero. Fang et al. (2011) derived the orbital periods of Beta and Gamma by performing simulations considering the triple system and Alpha's J_2 gravitational harmonic, and reported orbital periods of about 149.4 h for Beta and 16.46 h for Gamma. However, using the mentioned initial conditions for our simulations, the orbital period of Beta diverged from their reported orbital period. We used the Lomb–Scargle periodogram (Lomb 1976; Scargle 1982) and the searching ranges of [97, 200] and [10, 20] h for Beta and Gamma orbital periods, respectively. The output distance from Alpha and time were used to fit the periodogram model. The period considered for the periodogram calculations was the 2-yr integration and we obtained an orbital period of about 136.26 h for Beta when the three bodies were considered. However, when the orbital period is simply calculated using the third Kepler law, it matches the reported value (Fang et al. 2011). On the other hand, despite of the divergence of Beta's orbital period, the orbital period of Gamma did not diverge when we considered a three-body problem. This may be related to the fact that Gamma is closer to Alpha than Beta, thus Beta does not directly affect Gamma's orbit significantly. Nevertheless, according to Prado (2014) perturbation's map, the perturbation of Gamma is one order of magnitude larger than Beta's, and Gamma's perturbation is about ten times stronger for test particles orbiting Alpha, but close to Beta, thus Beta experiences some perturbation due to Gamma.

In order to measure how much the irregular shape of Alpha affects the orbits of Beta and Gamma, we simulated two scenarios: the standard case with Alpha as an oblate object (i.e. with the J_2 coefficient) and other with the irregular shape of Alpha (mascons case). Due to the complexity of modeling the mutual interaction between two irregularly shaped bodies, in our model we considered that the mascons of Alpha affect Beta, while the disturbance caused by Beta on Alpha corresponds to a point of mass interaction From Fig. 3 we see that the orbital radius of Beta does not suffer a change in its amplitude of oscillation due to Alpha's irregular shape. On the other hand, a different behaviour of the orbital radius of Gamma is noticed when the irregular shape is considered. The peak to peak amplitude of the orbital radius of Gamma in the standard case is about 40 m smaller than in the mascons simulation. The oscillation frequency of the orbital radius is also different, being 3.5 times larger for the mascons case when compared with the oblate model. Thus, the Alpha irregular shape does play an important role in the dynamics of Gamma, but does not significantly change the orbit of Beta.

We also ran a simulation to verify the perturbation of the irregular shape model of Beta, and no significant perturbation is noted in the orbit of Gamma. In summary, the main perturbation is caused by the irregular shape model of Alpha on the trajectory of Gamma.

3.2 Region 1

Given the initial conditions presented previously for region 1, the combination of semi-major axes and eccentricities resulted in 11 000 particles since they were considered 100 different particles for each (*a*, *e*) pair. Fig. 4 is a reproduction of fig. 2(a) from Araujo et al. (2012). It shows the stability diagram for the prograde particles and is coloured according to the surviving box percentage. The box with
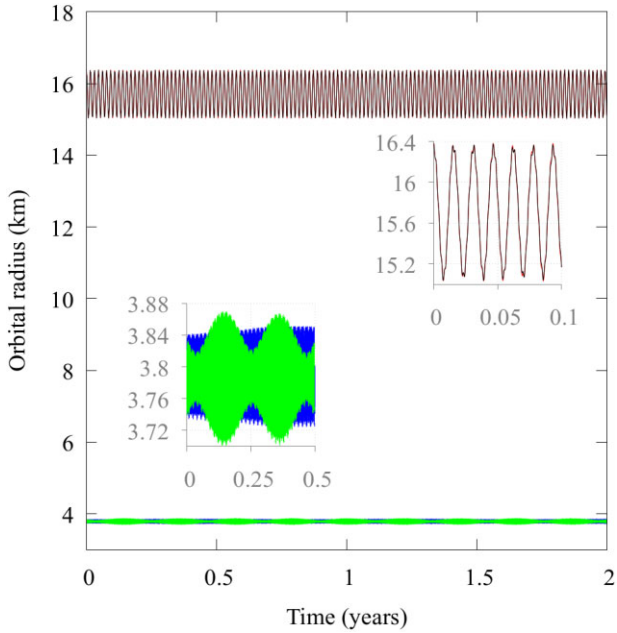
Figure 3. Orbital radius variation across time of Beta and Gamma for 2 yr. Considering the Alpha as a spherical body with the perturbation of its J_2 gravitational harmonic, the red and blue lines represent the orbital variation of Beta and Gamma, respectively. The black and green lines showed the orbital variation of Beta and Gamma, respectively, for the Alpha's irregular case scenario. The zoom in the figure shows the orbital radius of Gamma (inferior) and Beta (superior) for a period of six months.

a white triangle indicates 100 per cent of survival, and each box represents 100 particles. The full white line represents the collision line with Alpha for a radius of 1.3 km (approximately the Alpha volumetric radius is the same radius adopted by Araujo et al. 2012, 2015). The dashed line is the collision-line for a radius of 1.46 km (corresponding to Alpha upper altitude calculated on the body's surface; see Fig. 2). The dotted line represents the collision-line with Gamma. To compute these limits, we consider that the pericentre of the particle's orbit can not be smaller or equal to Alpha's radius, and the apocentre can not be larger or equal to Gamma's orbit. Hence, for the collision-line with Alpha we adopted $a \leq R_{\text{Alpha}}/(1 - e)$ and for Gamma's, $a \geq a_{\text{Gamma}}/(1 + e)$, where R_{Alpha} and a_{Gamma} are, respectively, the Alpha's radius and Gamma's semi-major axis.

In our simulations, we took into account only the irregular shape of Alpha. Since Gamma is much smaller (about a hundred times), its irregular shape will not significantly influence particles of region 1. The irregular shape of Beta was also not considered as its location is too far from region 1. For this prograde simulation, the results revealed that no particle survived for 2 yr. On the other hand, a massive quantity of particles was ejected or collided within just 7 d. The initial conditions with a semi-major axis higher than 2.4 km, near Gamma's orbit, were already unstable in Araujo et al. (2012) study. However, for values smaller or equal to 2.4 km, near Alpha's surface, there were many stable trajectories with $e \leq 0.25$ (Fig. 4). As we consider Alpha's shape, the irregularities destabilize all the remaining trajectories of region 1.

When retrograde particles are examined, an increase of survived particles occurs (Fig. 5). For the standard case, about 48 per cent of the particles survived for 2 yr of integration and, different from the prograde case (Fig. 4), the survived particles can reach a semi-major axis larger than 2.4 km and also larger eccentricities (Fig. 5a).


(a)
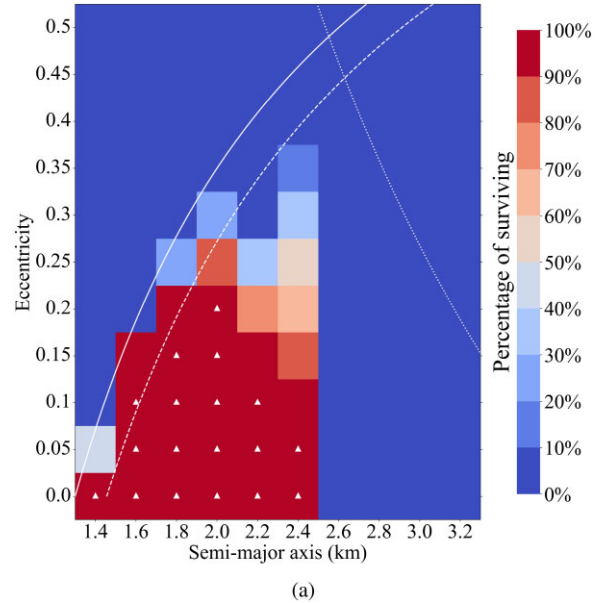
Figure 4. Diagram of the stability for region 1 for 2 yr considering prograde trajectories. The diagram is a reproduction of fig. 2(a) from the standard case (Araujo et al. 2012) with the triple system as points of mass and the J_2 of Alpha. Each box represents a set of 100 particles and the colour bar represents the percentage of surviving particles. The white triangles indicate 100 per cent of survival. The lines indicate the collision-lines with Alpha (full line for a radius of 1.3 km, dashed line for a radius of 1.46 km), and Gamma (dotted line, corresponding to the ejection distance).

However, the eccentricity did not exceed values larger than 0.4 for most survived particles. An interesting feature is a gap in the semi-major axis at 2.4 km. The particles with this semi-major axis have a 2:1 commensurability of mean motion with Gamma. The particles nearby this region suffer from a perturbation due to this resonance, and their eccentricity increase in such a way that they cross the collision line of the region (Araujo et al. 2015).

A decrease in the survived particles number and the ranges of semi-major axis and eccentricity was noticed when we consider the mascons case (Fig. 5b). The irregularities significantly affected the particles with pericentre closer to the central body. The gap in the 2.4-km semi-major axis is still present due to the 2:1 commensurability of mean motion with Gamma. This implies a resonance that also causes instability, and due to Alpha's irregular shape, this instability affects particles with initial eccentricities smaller than in the case of Fig. 5(a). Since their orbits can not reach larger values of eccentricities without colliding with Alpha or crossing the collision-line of Gamma, the boxes of initially almost circular orbits have a more significant percentage of survivors (Fig. 5b).

3.3 Region 2

The distribution of initial conditions in region 2 resulted in 50 600 particles between Gamma and Beta, where the orbits of Gamma and Beta correspond to collision lines that delimit the ejection of region 2. To calculate these lines, we assume that the pericentre of the particle's orbit cannot be smaller or equal to Gamma's semi-major axis and the apocentre larger or equal to Beta's semi-major axis. Fig. 6 shows the diagrams of stability of region 2 for the prograde case. For our simulations, we consider the irregular shapes of Alpha and Beta. A similar structure to the standard case (Fig. 6) still remains. The survived particles are also located in two preferential spots, but now
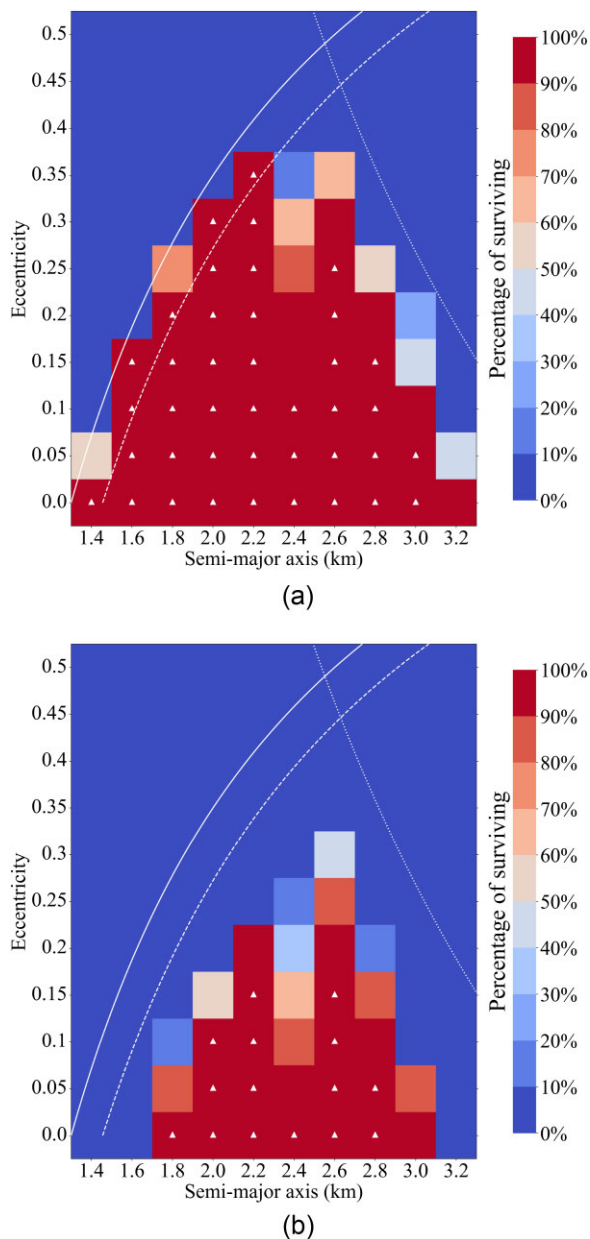
Figure 5. Region 1 stability diagram for 2 yr considering retrograde trajectories. Panel (a) is a reproduction of fig. 2(f) from the standard case (Araujo et al. 2015) and panel (b) shows the system considering the irregular shape of Alpha. Each box represents a set of 100 particles, and the colour bar represents the percentage of surviving particles. The white triangles indicate 100 per cent of survival. The lines indicate the collision with Alpha (full line for a radius of 1.3 km, dashed line for a radius of 1.46 km), and Gamma (dotted line corresponding to the ejection distance).

with semi-major axes near 6.9 km and 8.7 km, while for the standard case, they were concentrated around the semi-major axis of 7.3 and 9.5 km. The number of survivors decreased by about 67 per cent compared to the standard case. The elongated shape of Beta causes the removal of particles with a semi-major axis of 9.5 km, and a gap was formed at 7.7 km (Fig. 6b), dislocating in about 600 m from the gap formed in the standard case (Fig. 6a). These gaps are associated with a 3:1 mean motion resonance with Beta. Such resonance forces an increase in the eccentricities of the nearby particles destabilizing them and generating the gap.

For the mascons retrograde case, some regions were noticeably more disturbed than the standard case. The larger values of the semi-major axis became null for survivors due to the elongated shape of Beta (Fig. 7b), decreasing the initial semi-major axis stability border by about 800 m in comparison with the standard case (Fig. 7a). The (*a*, *e*) pairs with large eccentricities near Gamma and Beta collision lines did not reach a large percentage of survivors due to the instability caused by them, similar to the standard case. A prominent valley near the semi-major axis at 9.3 km was formed, and a minor one was also formed near 7.1 km (Fig. 7b). The major valley is associated with a 2:1 mean motion resonance with Beta and a 1:4 with Gamma. The combination of these resonances generated an instability that affected nearby particles with an initial eccentricity larger or equal to 0.2. In the minor valley exists a 3:1 mean motion resonance with Beta. It is interesting to note that the results of the standard case (Fig. 7a) were also found two valleys, but they were at different locations. Consequently, they were associated with resonances different from the ones described above.

3.4 Region 3

We set 15 400 initial conditions considering the range of *a* and *e*. The particles are orbiting Beta, and their motion is restricted by the collision-line of Beta and the distance of one Hill's radii of Beta with respect to Alpha (3.4 km). Fig. 8 shows the stability diagram for the prograde case for our reproduction of fig. 4(a) from Araujo et al. (2012). We obtained only five survived particles for the prograde case system with the Beta's shape model and Alpha as a spherical object. In contrast, for the standard case, most of the particles with a semi-major axis smaller than 1.4 km survive. Since five survived particles are not a considerable number for stability and considering that this case was already unstable without Alpha's shape model and the Sun tide, we did not explore their contribution to the stability of region 3. Unlike the standard case, we computed a more significant number of collided particles (about 57 per cent) and ejected particles (approximately 43 per cent). In addition, the particles near the Beta's surface were ejected or collided quickly, with about 78 per cent of the collisions and 69 per cent of the ejections in the first 7 d. Thus, the irregularities of Beta's shape cause extreme instability in the region.

For our mascons case, considering Beta's shape model and Alpha as a spherical body, we detected a decrease of 26.9 per cent of survived particles (Fig. 9b) for the standard case (Fig. 9a). The decrease of survivors occurred at the lower semi-major axis and larger eccentricities. The apocentre of the particles with a low semi-major axis and large eccentricities reach distances closer to Beta, giving rise to instability and, eventually, collisions and ejections. The collisions were about 38 per cent and 21.7 per cent for the ejections, where 57 per cent of these ejections and collisions occurred in the first 7 d. When we added Alpha's irregular shape model, we did not observe any significant changes (Fig. 9c). The statistics of survivors, collisions, and ejections were the same for both scenarios (with Alpha as a spherical body and with its irregular shape).

Fig. 10 presents the dimensionless parameters (see Hamilton & Krivov 1996; Moura et al. 2020) for more details) allowing us to compare the relative strength of each force (solar radiation pressure, Sun's tide, Alpha's gravity, and oblateness) according to the distance from Alpha. The Sun tide is represented by the colour green and Alpha's gravity and oblateness by the colours purple and blue, respectively. The colours orange, brown, and red represent the solar radiation pressure for a particle with a density of 1.0 g cm⁻³ and radius of 100 μm, 1 and 10 cm, respectively. Since the Alpha's oblateness in region 3 is about the same order of magnitude as the
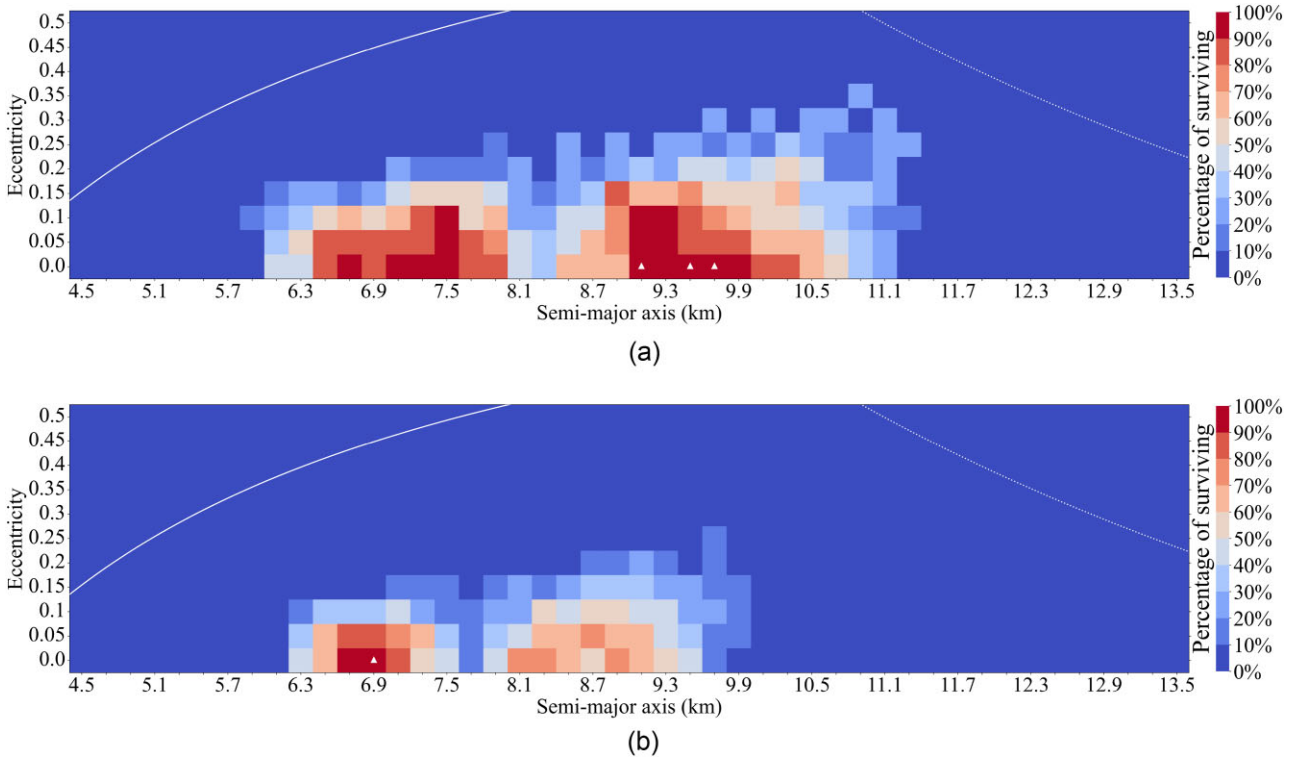
Figure 6. Diagram of the stability for region 2 for 2 yr considering prograde trajectories. Panel (a) is a reproduction of fig. 3(a) from the standard case (Araujo et al. 2012) and panel (b) shows the system considering the irregular shapes of Alpha and Beta. Each box represents a set of 100 particles, and the colour bar represents the percentage of surviving particles. The white triangles indicate 100 per cent of survival. The lines indicate the collision lines with Gamma (full line) and Beta (dotted line).

Sun tide (see Fig. 10), we concluded that the Sun's tidal perturbation may lower affect the region. Thus, we did not take into account this perturbation for the third region.

4 INSTABILITY DUE TO THE SOLAR RADIATION PRESSURE

Seeking a more realistic approach, we investigated how the solar radiation force changes the stability regions. The solar radiation pressure may cause an increase in the particle eccentricity and may change the stability presented previously. We performed numerical simulations changing the particle radius and preserving its density of $1.0 \, \mathrm{g \, cm^{-3}}$ (similar to the density of Alpha and Beta) to verify the size of the particles that can survive nearby the system. Thus, considering an area to mass ratio A, $\mathbf{R}$ as the vector Sun-particle, and R its module, the solar radiation pressure perturbation is given by (Scheeres & Marzari 2002)

$$\mathbf{a}_{\mathrm{srp}} = \frac{A G^* (1 + \eta)}{R^3} \mathbf{R}, \tag{1}$$

where $G^* = 1 \times 10^{17} \, \mathrm{kg \, m \, s^{-2}}$ is the solar constant in function of the solar luminosity and speed of light, and η is the reflectance of the particle. We consider a totally reflective material, thus $\eta = 1$. This work do not consider the shadowing effects, since, compared to the solar radiation pressure and the irregular gravitational perturbation, they are not significant to create a noticeable change in the survivors percentage.

Similarly to the Section 3, we used the N-BOM package to perform the simulations, but considering the solar radiation pressure (Valvano et al. 2022). We considered the same initial conditions for the three regions. We also choose a discrete distribution of the radius for the

particles to start in the order of centimeters (e.g. 10, 30, 50, 100, and 150 cm). We opted for a minimum radius of 10 cm due to the analyses of the dimensionless parameters of Fig. 10. As one can see, the perturbation of the radiation pressure on a particle smaller than 10 cm is high enough to generate instability and decrease the percentage of survivors. Thus, we simulated the system for 2 yr considering the retrograde case and our discrete particles radius.

4.1 Region 1

The irregularity of the central body causes considerable instability in region 1 compared to the standard case. For the total integration time of the prograde simulation, none of the particles has survived, and most of them have collided or ejected in just a few days (see Section 3.2). Thus, we did not perform a simulation with the solar radiation pressure for the prograde case since this perturbation will not generate any stability for the system. So, different from Sanchez & Prado (2019) results that found a stable region between Alpha and Gamma, when Alpha was modeled as a triaxial ellipsoid and Gamma as a spherical body, our results showed that region 1 was already unstable without the solar radiation pressure.

Fig. 11 shows the diagram of stability for region 2 considering the solar radiation pressure for the retrograde case for a particle with 10 cm of radius. The percentage of survivors for the simulation was 23 per cent and 15 pairs of (a, e) have 100 per cent of survival. The distribution of the percentage of survivors for the boxes is deeply similar to the case without the solar radiation pressure. We could see slight differences in percentage in specific boxes, but nothing significant. The gap in the semi-major axis of 2.4 km is still present and the 2:1 mean motion resonance with Gamma.
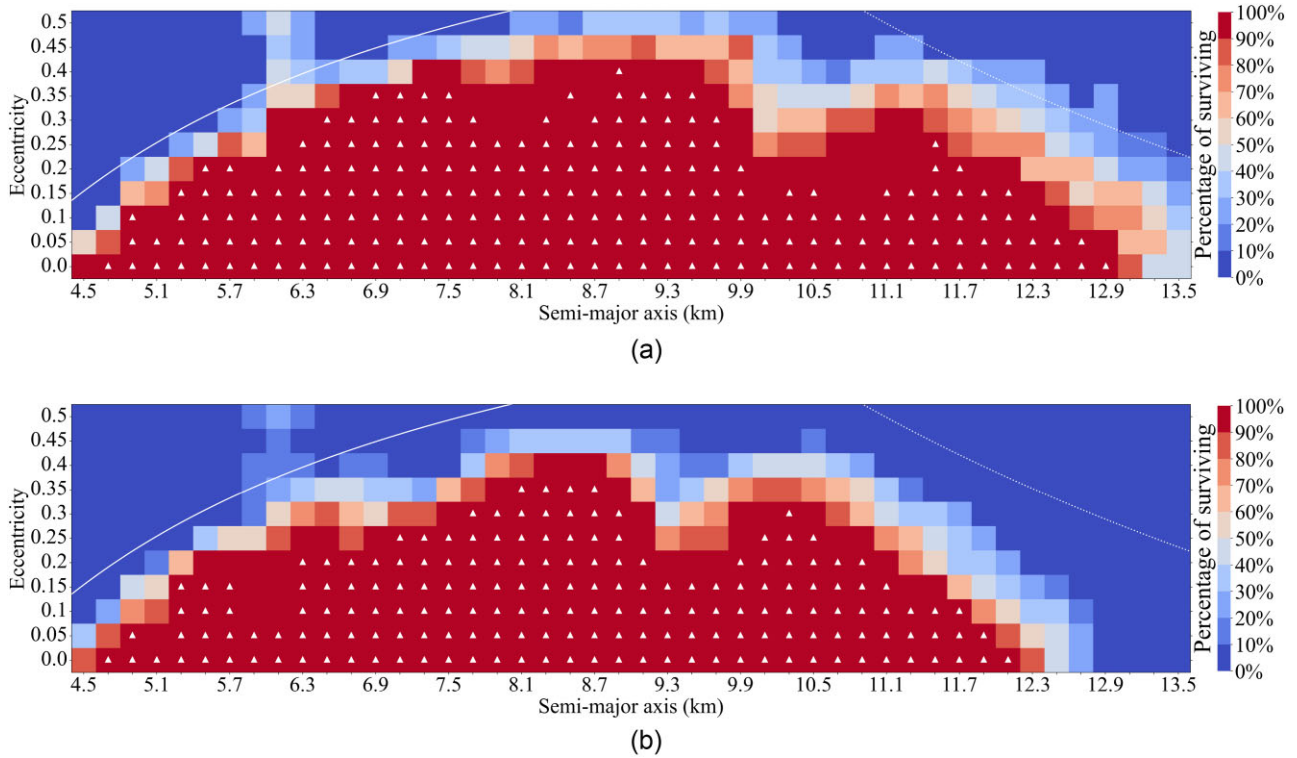
Figure 7. Diagram of stability for region 2 for 2 yr considering retrograde trajectories. (a) it is a reproduction of the bottom fig. 4 from the standard case (Araujo et al. 2015) and (b) shows the system considering the irregular shapes of Alpha and Beta. Each box represents a set of 100 particles and the colour bar represents the percentage of surviving particles. The white triangles indicate 100 per cent of survival. The lines indicate the collision-lines with Gamma (full line), and Beta (dotted line).
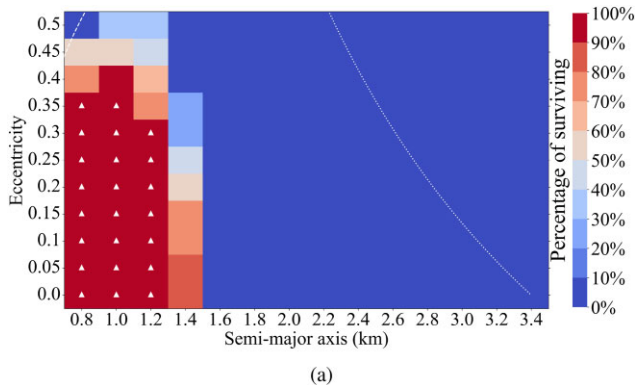
Figure 8. Reproduction of the diagram of the stability for region 3 for 2 yr considering prograde trajectories. The diagram is a reproduction of fig. 4(a) from the standard case (Araujo et al. 2012). Each box represents a set of 100 particles and the colour bar represents the percentage of surviving particles. The white triangles indicate 100 per cent of survival. The dashed line indicates the collision-line with Beta for a radius of 543 m. The dotted line corresponds to the Hill's radius of Beta with respect to Alpha and represents the ejection distance.

4.2 Region 2

If we consider a particle with a radius of 10 cm for the prograde case, no particle survived the effects of the solar radiation pressure for 2 yr. Although, when a radius of 30 cm was considered, about 2 per cent of the particles survived. However, no (*a, e*) pair presented 100 per cent stability. Thus, we increased the radius of the particles until we reached pairs with 100 per cent of stability. Increasing

the radius to 150 cm, we obtained a (*a, e*) pair with 100 per cent of stability and similar behaviour to the outcomes without the perturbation caused by the radiation (Fig. 12a). There are only two main regions of surviving particles, and the (*a, e*) pair with 100 per cent of survival was at the (6.7 km, 0.0) pair. Note that the size of the stability region was similar to the case without the radiation pressure, and the pair that reached 100 per cent of survival decreased by 200 m in the initial semi-major axis value (see Fig. 6b). The resonances near the semi-major axis of 7.7 and 8.1 km are still present.

For the retrograde case, considering particles with the minimum radius (10 cm) about 2 per cent of the particles survived the solar radiation perturbation. Increasing to 30 cm, about 13 per cent of the particles survived the entire simulation, but no (*a, e*) pair presented 100 per cent of survivors. Thus, we increased the radius of the particles to 50 cm. When this radius was considered, about 37 per cent of the particles survived, and boxes with 100 per cent of survival appeared (Fig. 12b). The location of the previous larger valley is now a gap that separates the regions of stability into two. The region of stability near Gamma (left-hand side from the gap) was the larger one and presented 30 pairs of (*a, e*) with 100 per cent of survival. Conversely, the second region of stability was smaller and presented no boxes with 100 per cent of survival. The resonances in the region of the previous larger valley are still observed. They appeared to be more effective in destabilizing the region with the addition of solar radiation pressure. We concluded the same for the 3:1 mean motion resonance with Beta as well as the resonance near the semi-major axis of 6.1 km. The 1:3 mean motion resonance with Gamma was also preserved but did not create a delimited valley as the previously mentioned resonances.
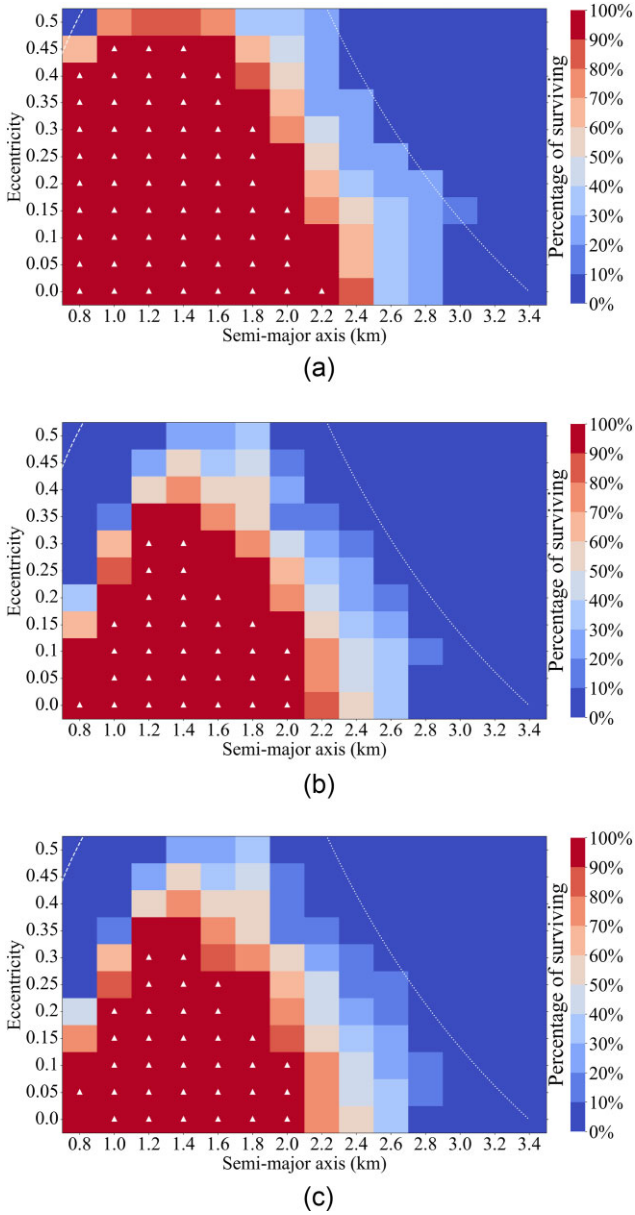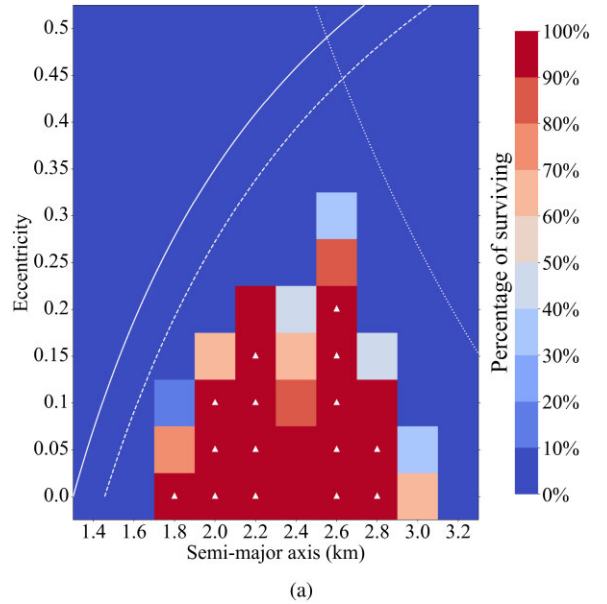
Figure 9. Diagram of the stability for region 3 for 2 yr considering retrograde trajectories. Panel (a) is a reproduction of fig. 6(f) from the standard case (Araujo et al. 2015); panel (b) shows the system considering the irregular shape of Beta; and panel (c) considers the irregular shapes of Alpha and Beta.Each box represents a set of 100 particles and the colour bar represents the percentage of surviving particles. The white triangles indicate 100 per cent of survival. The dashed line indicates the collision-line with Beta for a radius of 543 m. The dotted line corresponds to the Hill's radius of Beta with respect to Alpha and represents the ejection distance.

4.3 Region 3

The prograde case around Beta was already unstable without the solar radiation pressure. Thus, we did not simulate this region with this additional perturbation since it cannot produce any stability in the region. Considering that the effect of Alpha's shape model was not relevant to region 3, we did not consider its shape model to perform the simulations with solar radiation pressure for the retrograde case. For the initial radius of 10 cm, about 9 per cent of the particles survived the entire simulation, and only one (a, e) pair reached 100 per cent of survival. The majority of the particles that
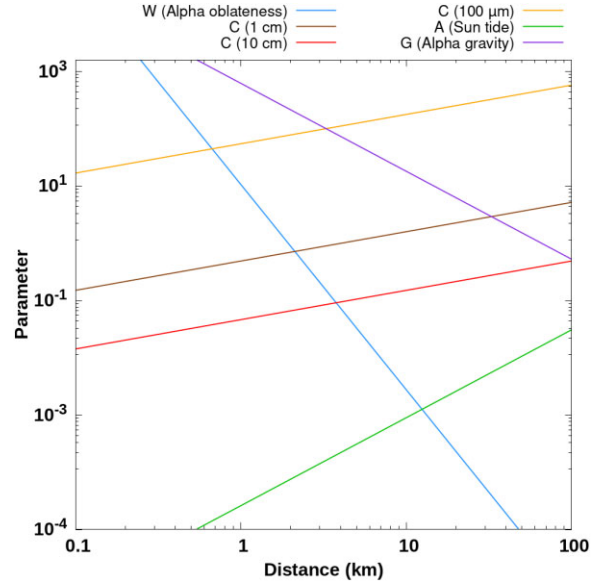
Figure 10. Variation of the dimensionless parameters Sun tide (green), the solar radiation pressure for a particle with a radius of 100 μm (orange), 1 (brown) and 10 cm (red), Alpha's oblateness, and gravity (blue and purple, respectively).

Figure 11. Diagram of the stability for region 1 for 2 yr considering retrograde trajectories for particles with 10 cm of radius and the perturbation of solar radiation pressure. The irregular shape of Alpha was considered for this system. Each box represents a set of 100 particles and the colour bar represents the percentage of surviving particles. The white triangles indicate 100 per cent of survival. The lines indicate the collision-lines with Alpha (full line for a radius of 1.3 km, dashed line for a radius of 1.46 km), and Gamma (dotted line corresponding to the ejection distance).

survived were near Beta and with low eccentricities, being the box of 100 per cent of survival with the initial condition of (800 m, 0.0). Increasing the radius to 30 cm, the number of survived particles was about three times larger, and the region of stability almost reached half of the Hill's radius (Fig. 13). Similar to the case without the solar radiation pressure, larger eccentricities did not produce stability. The stables (a, e) pairs have eccentricities smaller than 0.2.
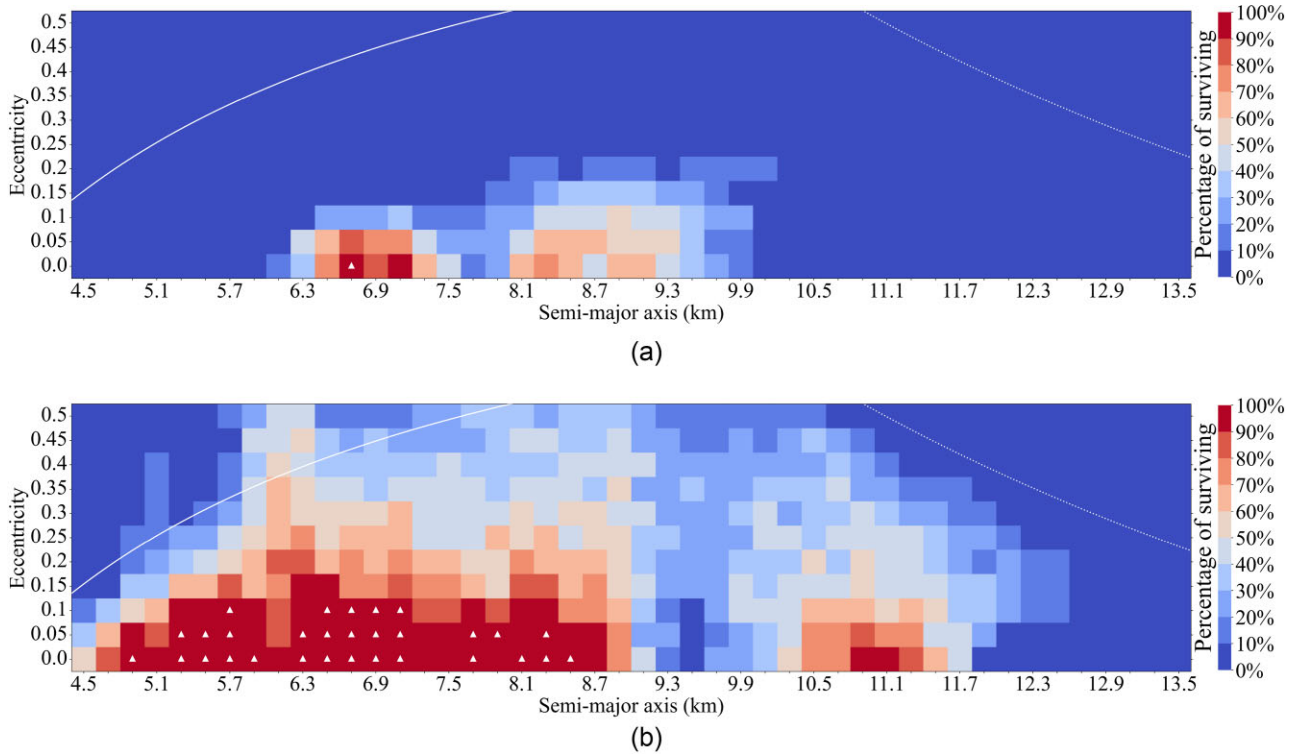
Figure 12. Diagram of stability for region 2 for 2 yr considering (panel a) prograde and (panel b) retrograde trajectories for particles with radii of 150 and 50 cm, respectively. The irregular shapes of Alpha and Beta were considered for this system. Each box represents a set of 100 particles and the colour bar represents the percentage of surviving particles. The white triangles indicate 100 per cent of survival. The lines indicate the collision-lines with Gamma (full line), and Beta (dotted line).

5 LONG-PERIOD SIMULATIONS

Considering the stability of a spacecraft, such as the ASTER mission spacecraft, for example, 2 yr of stability in the regions would be sufficient for executing a mission. However, 2 yr is a short time for natural materials, such as fragments and small rocks. Thus, we performed simulations for 2000 yr for the survived particles presented in Section 3 (without the solar radiation pressure). Since natural material is in retrograde orbits requires an improbable process such as gravitational capture have occurred. Therefore, we did not study the retrograde case for a long time.

Once the prograde regions 1 and 3 were already unstable for 2 yr, we only simulated region 2 for 2000 yr to verify its long-term stability. Considering the survivors of region 2, about 94 per cent of them collided or were ejected in the first 90 yr, and all of them became unstable before 2000 yr. Thus, we did not include the solar radiation pressure in the system since it was already unstable.

6 FINAL COMMENTS

The main goal of this work was to improve the determination of the stability regions in the triple system 2001 SN₂₆₃ found in the works Araujo et al. (2012), Araujo et al. (2015). The advances were made considering more realistic gravitational perturbations due to the bodies' irregular shapes and taking into account the solar radiation pressure.

For the prograde region 1, the irregular shape of Alpha was sufficient to destabilize the entire region. For the retrograde scenario, 24 per cent of the particles survived the 2 yr of simulation, which is about half the survivors of the case without the irregularities
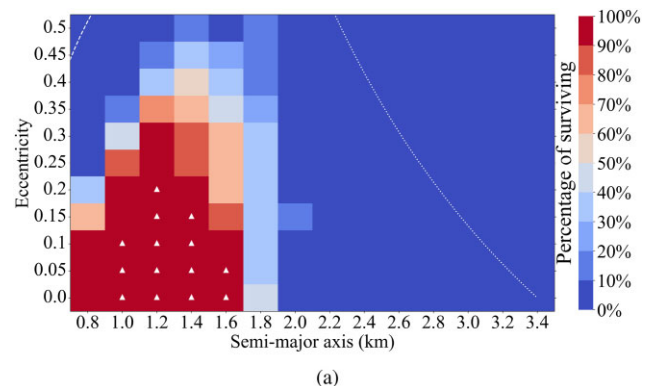
Figure 13. Diagram of stability for region 2 for 2 yr considering retrograde trajectories for particles with radius of 30 cm. The irregular shape of Beta was considered for this system. Each box represents a set of 100 particles and the colour bar represents the percentage of surviving particles. The white triangles indicate 100 per cent of survival. The dashed line indicates the collision-line with Beta for a radius of 543 m. The dotted line corresponds to the Hill's radius of Beta with respect to Alpha and represents the ejection distance.

of Alpha's shape model (Araujo et al. 2015). Different from the prograde case of region 1, the prograde scenario of region 2 presented about 6.7 per cent survivors, and only one (a, e) pair reached 100 per cent of survival. A valley separated the regions of stability in two spots, and in this valley, we found a 3:1 mean motion resonance with Beta. The retrograde case presented about 8.5 times more survivors than the prograde case, and the outcomes with and without the irregular shape models are slightly different. The irregular shape

of Beta causes more instability at the end of the region, and the main valley becomes more noticeable. Some resonances were also found in this region.

Similar to the prograde scenario of region 1, the prograde case of region 3 has no stability. This result was obtained by only considering the irregular shape of Beta. In the same way, we performed the retrograde case. We detected about 40.3 per cent of surviving and 31 pairs of (a, e) reached 100 per cent of survival. Adding the Alpha's shape model, the statistic was basically the same. Thus, we conclude that since the third region is far from Alpha. Its irregularities did not significantly affect the particles around Beta. Considering this, we did not add the Sun tide to the system since its order magnitude in this region is similar to the Alpha's oblateness.

The solar radiation pressure plays an important role in the stability of particles in the system and may produce a significant perturbation in the particles' evolution. For this reason, we searched, for each region, the order of magnitude of the radius of the particles that could survive this perturbation. The prograde case of regions 1 and 3 was already unstable without the solar radiation pressure, so we did not simulate these scenarios. For retrograde region 1, 23 per cent of the particle with a radius of 10 cm were able to survive. On the other hand, 24.4 per cent of the retrograde particles with a radius of 30 cm survived in region 3. For the vast region 2, a particle's radius of at least 50 cm for the retrograde case and 150 cm for the prograde case was necessary. However, we identified surviving for a particle with a radius of 30 cm for the prograde case, but it was three times smaller and with no box with 100 per cent of survival. In short, the only prograde case scenario capable of surviving was region 2. The particle radius of the retrograde case was one order of magnitude smaller, and the three regions had survivors. Hence, the retrograde scenario was the most stable and may be a safer choice for a spacecraft.

Since 2 yr are too short for fragments and small rocks to verify stability, we performed a 2000 yr of simulation. We only considered the prograde case. For regions 1 and 3, we did not simulate as they were already unstable for 2 yr. Besides, for region 2, none of the particles survived for 2000 yr of integration. Hence natural objects, such as fragments and small rocks, are unlikely to exist in regions 1, 2, and 3.

Our discussion about the stability around the three regions of the triple system (153591) 2001 SN_{263} might contribute to the planning of the ASTER mission. Furthermore, it may help understand the dynamics of triple systems and perhaps the planning of other future missions.

DATA AVAILABILITY

The data underlying this paper will be shared upon reasonable request to the corresponding authors.

REFERENCES

Araujo R. A. N., Winter O. C., Prado A. F. B. A., Sukhanov A., 2012, MNRAS, 423, 3058
Araujo R. A. N., Winter O. C., Prado A. F. B. A., 2015, MNRAS, 449, 4404
Becker T. M. et al., 2015, Icarus, 248, 499
Borderes-Motta G., Winter O. C., 2017, MNRAS, 474, 2452
Carry B., 2012, Planet. Space Sci., 73, 98
Cheng A. et al., 2016, Planet. Space Sci., 121, 27
Fang J., Margot J. L., Brozovic M., Nolan M. C., Benner L. A. M., Taylor P. A., 2011, AJ, 141, 154
Flynn G. J., Consolmagno G. J., Brown P., Macke R. J., 2018, Geochemistry, 78, 269
Fujiwara A. et al., 2006, Science, 312, 1330
Geissler P., Petit J. M., Durda D. D., Greenberg R., Bottke W., Nolan M., Moore J., 1996, Icarus, 120, 140
Hamilton D. P., Krivov A. V., 1996, Icarus, 123, 503
Harris A. W., Fahnestock E. G., Pravec P., 2009, Icarus, 199, 310
Hirabayashi M. et al., 2020, Icarus, 352, 113946
Kawaguchi J., Fujiwara A., Uesugi T., 2008, Acta Astronaut., 62, 639
Lauretta D. et al., 2015, Meteorit. Planet. Sci., 50, 834
Lauretta D. et al., 2017, Space Sci. Rev., 212, 925
Lomb N. R., 1976, Ap&SS, 39, 447
Macke R. J., Consolmagno G. J., Britt D. T., 2011, Meteorit. Planet. Sci., 46, 1842
Marchis F. et al., 2012, Icarus, 221, 1130
Michel P. et al., 2020, Nat. Commun., 11, 1
Moura T., Winter O., Amarante A., Sfair R., Borderes-Motta G., Valvano G., 2020, MNRAS, 491, 3120
Müller T. et al., 2017, A&A, 599, A103
Ostrowski D., Bryson K., 2019, Planet. Space Sci., 165, 148
Perna D., Alvarez-Candal A., Fornasier S., Kaňuchová Z., Winter S. G., Neto E. V., Winter O., 2014, A&A, 568, L6
Prado A. F., 2014, Adv. Space Res., 53, 877
Prockter L., Murchie S., Cheng A., Krimigis S., Farquhar R., Santo A., Trombka J., 2002, Acta Astronaut., 51, 491
Rubincam D. P., 2000, Icarus, 148, 2
Sánchez P., Scheeres D. J., 2016, Icarus, 271, 453
Sanchez D. M., Prado A. F., 2019, J. Spacecr. Rockets, 56, 1775
Scargle J. D., 1982, ApJ, 263, 835
Scheeres D., Marzari F., 2002, J. Astronaut. Sci., 50, 35
Sukhanov A. A., de C. Velho H. F., Macau E. E., Winter O. C., 2010, Cosm. Res., 48, 443
Valvano G., Winter O. C., Sfair R., Machado Oliveira R., Borderes-Motta G., Moura T., 2022, MNRAS, 510, 95
Vernazza P. et al., 2015, ApJ, 806, 204
Veverka J. et al., 2000, Science, 289, 2088
Walsh K. J., 2018, ARA&A, 56, 593
Walsh K. J., Richardson D. C., Michel P., 2008, Nature, 454, 188
Winter O., Valvano G., Moura T., Borderes-Motta G., Amarante A., Sfair R., 2020, MNRAS, 492, 4437
Yoshikawa M., Kawaguchi J., Fujiwara A., Tsuchiyama A., 2015, Asteroids IV. Univ. Arizona Press, Tucson, AZ

This paper has been typeset from a TeX/LaTeX file prepared by the author.